Proceedings of the ASME 2022 International Design Engineering Technical Conferences and Computers and Information in Engineering Conference IDETC/CIE 2022 August 14-17, 2022, St. Louis, Missouri, USA

DETC2022-89856

DESIGN AND MODELING OF A NEW VARIABLE STIFFNESS ROBOTIC FINGER BASED ON RECONFIGURABLE BEAM PROPERTY CHANGE FOR FLEXIBLE GRASPING

Wei Xu, Jiaming Fu, Dongming Gan*
Purdue Polytechnic Institute, Purdue University, West Lafayette, Indiana 47907

ABSTRACT

Flexible grippers can provide fine grasping and manipulation to various objects and environment interactions. However, most current mechanisms can not change the stiffness in a short time, which limits the application scenario of the flexible grippers. This paper presents a novel variable stiffness robotic finger that can adapt to soft and rigid gripping objects by continuously changing its stiffness over a wide range in a short period of time. The principle is to change the second area moment of inertia of the finger by changing the filling ratio of the cavity between two parallel beams. A complete theoretical stiffness model is developed and compared with the finite element analysis (FEA) model. Effects of multiple design parameters on finger stiffness performance are compared and analyzed, and the accuracy of the theoretical model is verified, with a maximum error of less than 6.5%. The performance of the finger is further evaluated through an experimental prototype, which proved that the finger can safely perform a wide range of daily object-grasping tasks with adaptable compliance. The proposed stiffness-varying mechanism can adjust stiffness in a short time with a very large ratio (around 1:37). The design provides a new direction in developing variable-stiffness robotic grippers for flexible grasping.

Keywords: Variable Stiffness Robotic Finger, Reconfigurable Beam, Compliant Structures, Stiffness Modeling

1 INTRODUCTION

Robotic grippers [1, 2] are increasingly important for robots, but most robotic grippers consist mainly of a set of rigid joints and beams, resulting in a lack of flexibility when grasping. This makes it difficult for robots to adapt to some working conditions, especially for human-robot interaction. In recent years, soft robots have been favored by researchers because of their good adaptability [3], compliance [4], and safety [5], especially for soft robotic grippers [6, 7]. Compared with a rigid robotic gripper, a soft robotic gripper has significant advantages. It not only is safer when it collides with humans [8], but also can better adapt to the shape and position of objects to achieve the gripping of fragile and fragile objects [9, 10]. However, soft robotic grippers also have shortcomings such as small contact force, low positioning accuracy, complex motion model, and high control difficulty [11]. Variable stiffness robotic grippers can solve the above problems by actively adjusting their stiffness according to the condition of operating in a wide range of applications [12].

One method to design variable stiffness grippers is to incorporate variable stiffness materials such as shape-memory polymer [13], composite materials [14], magnetorheological fluid [15, 16], and dielectric elastomer [17]. Al-Rubaii et al. [18] proposed a flexible pneumatic actuator using conductive polylactic for stiffness and shape adjustment, and developed a gripper using two pneumatic actuators. Firouzeh et al. [19] changed the elastic modulus of the finger by changing the temperature to achieve the glass transition of the shape-memory polymer. Al-Abeach et al. [20] proposed the application of the McKibben muscle to design a gripper, whose fingers consists of three

^{*}Correspondence: dgan@purdue.edu

contractile muscles surrounding an expansile muscle, and when pressure is applied, the two types of muscles form an antagonistic action, thus increasing the stiffness of the fingers without causing a change in position. However, this method has the problems of small range of stiffness, small driving force, complex assembly, and poor controllability.

Another method is by changing the mechanical structure property, which has performed promising results [21]. Kim et al. [22] proposed a layer interference variable stiffness principle using negative pressure to change interlayer friction and developed a variable stiffness serpentine gripper based on this principle. Li et al. [23] designed a novel passive particle interference principle to achieve variable stiffness. When inflating the soft body actuator, the soft body actuator expands and causes the particles in the cavity to squeeze each other, thus improving the overall structural stiffness. Chandrasekaran et al. [24] proposed a variable stiffness gripper using the concept of stability of truss structures. This design is able to partially conform to the surface of the grasped object and rapidly change its stiffness using compliant rotating elements embedded inside. Li et al. [25] developed a variable stiffness gripper by rotating a built-in hinge shaft to change the effective second area moment of inertia of the gripper. Its stiffness can be varied continuously. Melchiorri et al. [26] designed a gripper with a flexible material covering the surface of the main structure, which is driven by a twisted string actuation. Two springs twist around each other, and the total length is smaller due to spring winding and a passive change in the stiffness of the gripper while driving. The super-redundant variable stiffness gripper developed by Kim et al. [27] consists of many specifically shaped rings and wire cords assembled in series, with flexible washers fitted between two adjacent rings. The stiffness of the gripper can be changed by adjusting the preload force of the wire cords in a specific direction, and the stiffness is approximately linear to the preload force. This method still has a limited range of the stiffness adjustment.

To develop grippers with a large range of stiffness change ratio, this paper proposes a new finger design through a reconfigurable parallel beam mechanism. It can adapt to multiple gripping tasks without changing the finger. The stiffness of the finger is controlled by the mechanical structure changes. A movable slider is placed between two flexible sheets to change the stiffness of the finger continuously by changing the position of the slider. The process of stiffness adjustment is simplified by simple mechanical input to make it fast and accurate. The stiffness can be changed by tens of times in a short time. Stiffness adjustment and finger movement are independent of each other. The stiffness adjustment performance of the finger is comprehensively investigated by comparing and combining theoretical models, finite element analysis (FEA), and experimental tests. The wide applicability of this design is demonstrated.

2 CONCEPT OF THE DESIGN

The structure of the gripper is shown in Fig. 1. It consists of two fingers. For each finger, its exterior is made of two parallel beams. and its interior has a slider that can move in the axial direction. The stiffness of the finger can be changed by changing the ratio of the slider filling the internal cavity. When the filling ratio is lowest, the finger stiffness is minimum, and when the slider fills the cavity, the finger stiffness is maximum. The filling changes the second area moment of inertia and the ratio of the hollow beam over solid beam of the parallel beam mechanism and correspondingly its output stiffness. The slider can be driven by a stepper motor to change the stiffness continuously. In order to keep the fingers in one piece when deformation occurs, a restrictor is provided at the head of the slider, so that the slider and the flexible sheets remain tightly attached.

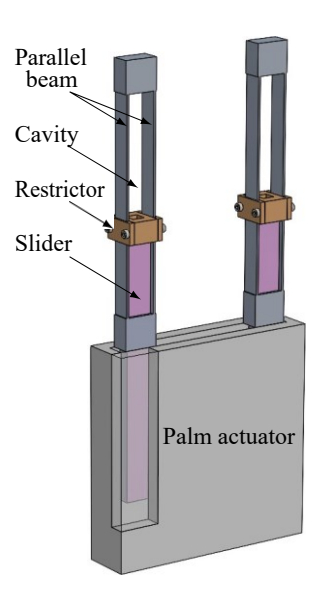


FIGURE 1. THE STRUCTURE OF THE GRIPPER.

3 STIFFNESS MODELING OF THE FINGER MECHA-NISM

In this section, a comprehensive stiffness model is developed based beam superposition principle and compared with FEA model.

3.1 Theoretical Stiffness Modeling

A parametric model of the proposed variable stiffness finger mechanism is shown in Fig. 2. The finger can be divided into three main parts, a solid part S_aS_b at the finger tip that contacts

with grasped objects, a flexible part S_bS_c in the middle and a solid part S_cS_d at the bottom [28]. Section S_d is fixed in the palm of the robot gripper. The effective height of the finger is unified as H and the effective thickness is unified as B. Note that the thickness of the slider is slightly less than the thickness of the parallel beam, which is simplified here for calculation convenience. The lengths of the head and root parts are L_h and L_r respectively. The length of the cavity part is L_c . A ratio, λ , of the cavity filled by the slider is introduced. The range of the slider-filling ratio λ is 0.1 to 1.0. When $\lambda = 0.1$, the slider is at the rightmost end. The proportion of the cavity is highest. But since the restrictor still needs some space, λ is greater than 0. When $\lambda = 1.0$, the slider is at the leftmost end and the entire cavity is filled. The lengths for the S_aS_b , S_bS_c and S_cS_d parts are L_h , (1 λ) L_c and λ $L_c + L_r$ respectively. When a force F is applied to the section S_a , the finger deforms. The deformation in the thickness direction will be ignored because it is very small relative to the deformation in the direction of force F [29]. In the direction of F, the deflection is greater in the S_bS_c part, and the deflection in the S_aS_b and S_cS_d parts are small, but should not be ignored. Because they have a certain thickness, their elasticity has a significant impact on the accuracy of the model.

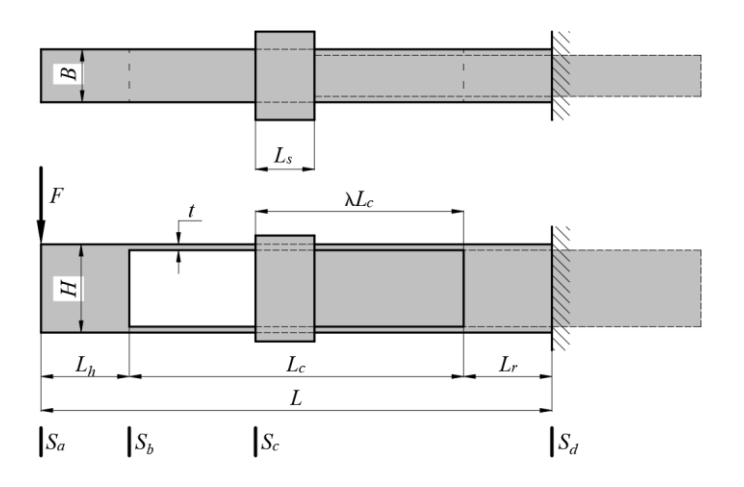


FIGURE 2. PARAMETRIC MODEL OF THE FINGER.

The moment of inertia of the S_aS_b and S_cS_d parts is

$$I_t = I_b = \frac{H^3 B}{12} \tag{1}$$

The thickness of the middle flexible sheet is t. The moment of

inertia of the S_bS_c part is

$$I_m = \frac{t^3 B}{12} \tag{2}$$

Depending on the moment of inertia, the deflection of the three parts of the finger is calculated segment by segment. Then the results are finally combined together to obtain the total deflection of each part acting on section S_a .

Firstly S_bS_c and S_cS_d parts are assumed as rigid bodies, meaning they are fixed and can not deform. Then the deflection angle ϑ_a and displacement δ_a of the section S_a with respect to the other two parts are

$$\theta_a = \frac{\hat{FL}_h^2}{2EI_t} \tag{3}$$

$$\delta_a = \frac{FL_h^3}{3EI_t} \tag{4}$$

where E is Young's modulus. Secondly, S_aS_b and S_cS_d parts are assumed as rigid bodies. The deflection only occurs in the S_bS_c part. It is affected by the force conducted from the S_aS_b part. According to the theory of the parallel guide mechanism [30], the deflection angle in S_bS_c part also affects the deformation of section S_a . Then superimposed on the deformation of the S_bS_c part, the total contribution of the deformation of S_bS_c part to the deformation of section S_a can be obtained. The deflection angle ϑ_b and displacement δ_b of the middle part are

$$\theta_b = \frac{t^2}{6(H - 2t)^2} \left\{ \frac{FL_h[(1 - \lambda)L_c]}{EI_m} + \frac{F[(1 - \lambda)L_c]^2}{2EI_m} \right\}$$
 (5)

$$\delta_{ab} = \theta_b L_h \tag{6}$$

$$\delta_b = \frac{F[(1-\lambda)L_c]^3}{24EI_m} \tag{7}$$

Then S_aS_b and S_bS_c parts are assumed as rigid bodies. The S_cS_d part is affected by force F and generates a deflection angle $\vartheta_{c,f}$ and displacement $\delta_{c,f}$. In addition, the effect of the bending moment $F[L_h + (1 - \lambda)L_c]$ can not be ignored. It can produce a

deflection angle ϑ_{cm} and a displacement δ_{cm} . These eventually are transmitted to section S_a , causing deformation.

$$\theta_{cf} = \frac{F(L_r + \lambda L_c)^2}{2EI_b^2} \tag{8}$$

$$\delta_{cf} = \frac{F(L_r + \lambda L_c)^3}{3EI_b^2} \tag{9}$$

$$\theta_{cm} = \frac{F[L_h + (1 - \lambda)L_c](L_r + \lambda L_c)}{EI_h^2}$$
 (10)

$$\delta_{cm} = \frac{F[L_h + (1 - \lambda)L_c](L_r + \lambda L_c)^2}{2EI_h^2}$$
 (11)

$$\delta_{ac} = (\theta_{bf} + \theta_{bm})[L_h + (1 - \lambda)L_c]$$
(12)

$$\delta_c = \delta_{cf} + \delta_{cm} \tag{13}$$

Finally, the above displacements acting on section S_a are added up to obtain the total displacement.

$$\delta = \delta_a + \delta_{ab} + \delta_b + \delta_{ac} + \delta_c \tag{14}$$

Then the stiffness is

$$k = \frac{F}{\delta} \tag{15}$$

3.2 Finite Element Analysis Modeling

In order to verify the accuracy of the theoretical model and to investigate the effect of various design parameters on finger performance, an FEA method was performed using ANSYS. In the model, section S_d of the finger is fixed, and a force is applied at section S_a . Mesh size is set as 1 mm, as shown in Fig. 3(a). In the example in Fig. 3(b), the filling ratio λ , is chosen at the average of the maximum and minimum values, giving $\lambda=0.55$. The applied force F is 2 N after testing the load capacity of the designed finger mechanism. It can be seen that the finger deformation occurs as expected. The deformation of the cavity part is large while that of the slider filling part is small. The deformation was recorded and used to calculate stiffness k divided by the applied force F, which is compared with the theoretical value in the following section.

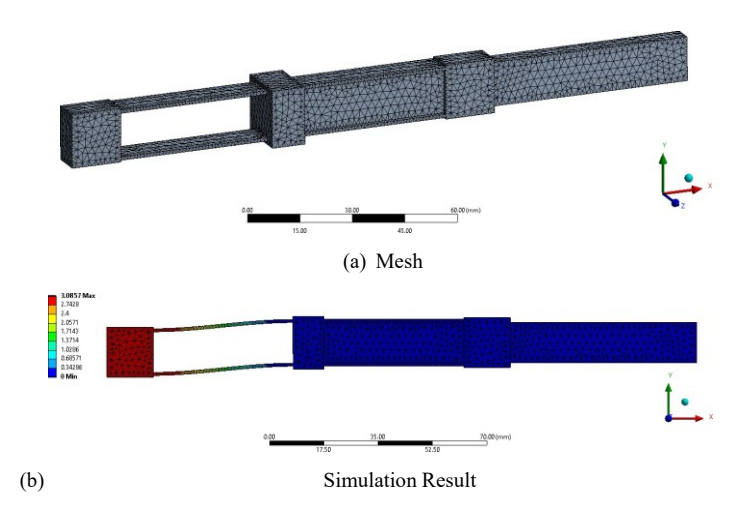


FIGURE 3. FEA MODEL.

3.3 Stiffness Variation and Comparison Between the Theoretical Model and FEA

The parameters to explore are shown in Tab. 1. The key parameters include the finger height H, thickness B, parallel beam thickness t, and cavity length L_c . When one of these parameters is changed, the other parameters remain unchanged.

TABLE 1. KEY PARAMETERS.

Parameters (mm)	Group 1	Group 2	Group 3	Group 4
Н	11~19	15	15	15
t	1	0.6~1.4	1	1
B	9	9	5~ 13	9
L_c	100	100	100	60~ 140
L_h	15	15	15	15
L_r	15	15	15	15

The performance of the finger with different parameters is shown in Fig. 4. It can be seen that the stiffness of the finger increases with the height of the finger H, the thickness of the flexible sheet t, and the thickness of the finger B, and decreases with the length of the cavity part L_c . The trend of deformation is opposite to that of stiffness. The stiffness is more sensitive when H is small, as shown in Fig. 4(a). This is because it is difficult for the deformation of the non-cavity part to affect the total deformation when H is large. The stiffness is more sensitive

when t is large, as shown in Fig. 4(c). Because its contribution to the total stiffness becomes increasingly non-negligible when t is large. The relationship between the thickness B and the stiffness is linear, as shown in Fig. 4(e). The stiffness is more sensitive when L_c is small, as shown in Fig. 4(g). The lengths of the head and root parts, L_h and L_r , are fixed. The cavity part contributes more to the deformation. When L_c is small, the proportion of the cavity part L_c/L is small, and the stiffness is more sensitive.

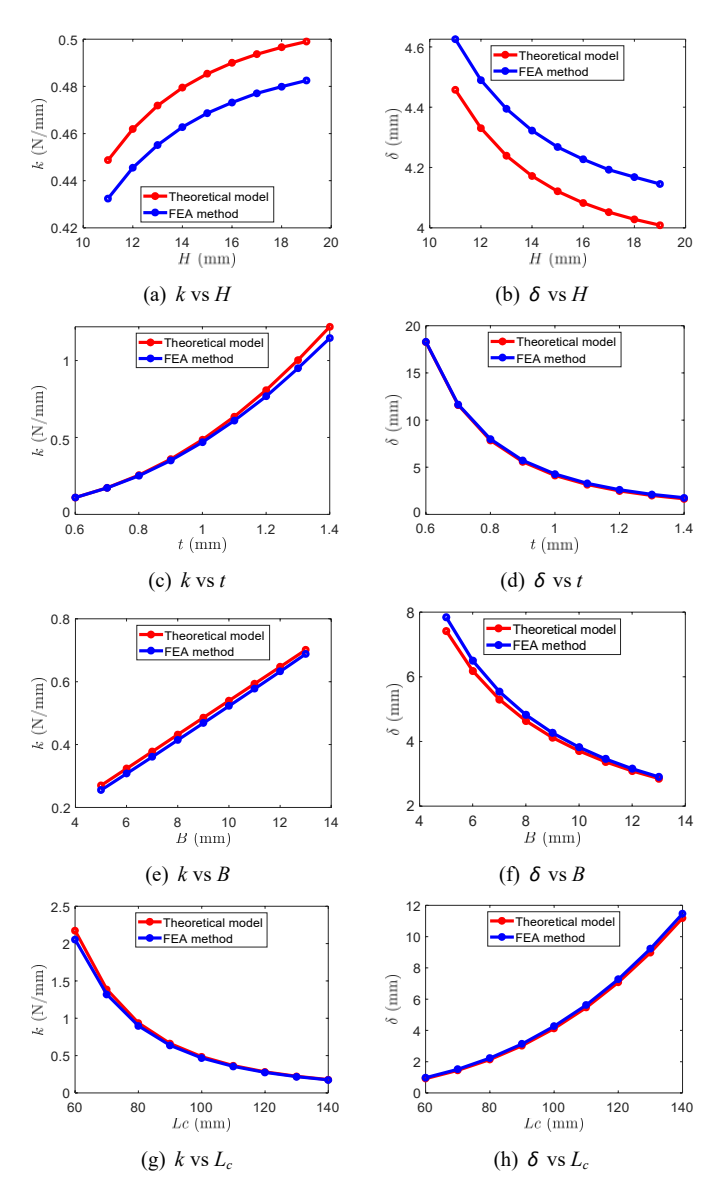


FIGURE 4. STIFFNESS AND DEFORMATION VARYING WITH DIFFERENT DESIGN PARAMETERS

A comparison of the two methods shows that the theoretical method yields a greater stiffness for a general given condition.

Using the FEA results as a benchmarks, errors of the theoretical model e with different parameters are shown in Fig. 5. The maximum error occurs when t=1.4 mm, reaching 6.44% which quite low in compliant mechanism analysis. This result verifies the accuracy of the theoretical model.

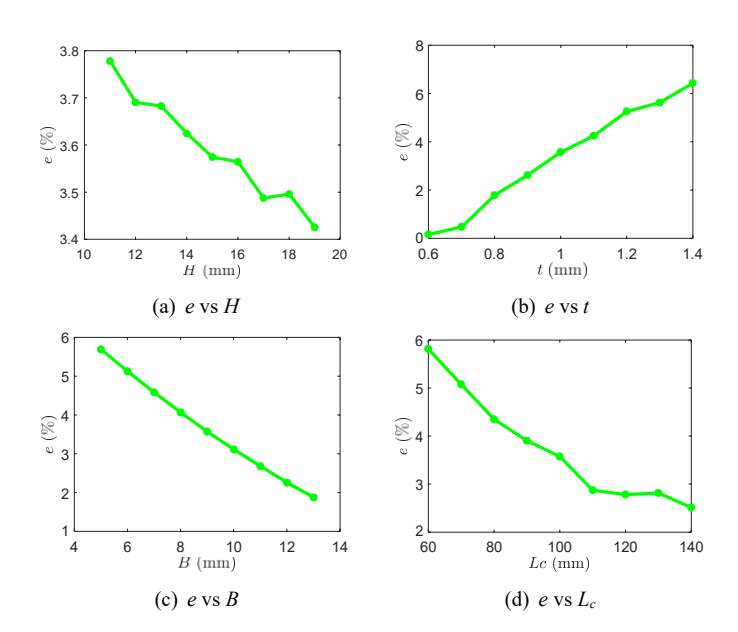


FIGURE 5. ERROR VARYING WITH DIFFERENT DESIGN PARAMETERS

4 PROTOTYPE AND EXPERIMENTAL VALIDATION

In this section, a finger prototype is introduced for experimental test, and a demonstration is done to show the application scenarios of the finger.

4.1 Stiffness Performance of the Experimental Prototype

3D printing method was used to produce the finger prototype. Based on a general gripper dimension estimation and the previous theoretical analysis, design parameters of the finger are selected as in Tab 2. The printing material is polylactic acid, and the infill parameter is 60%. Its Young's modulus *E* is 2600 MPa by experimental measurement. MARK-10 ESM303 Motorized Tension/Compression Test Stand was used to obtain the force and deformation of the finger as shown in Fig. 6. The root of the finger is fixed on the vise, and the other end is free to apply the simulated contact forces by the tester probe moving from up to down. To avoid overloading the test piece, the applied force is up to 3 N. The force and travel distance were recorded during this process for stiffness calculation.

TABLE 2. FINGER PARAMETERS.

Parameters (mm)	value	
Н	15	
t	1	
В	9	
L_c	100	
L_h	15	
L_r	15	

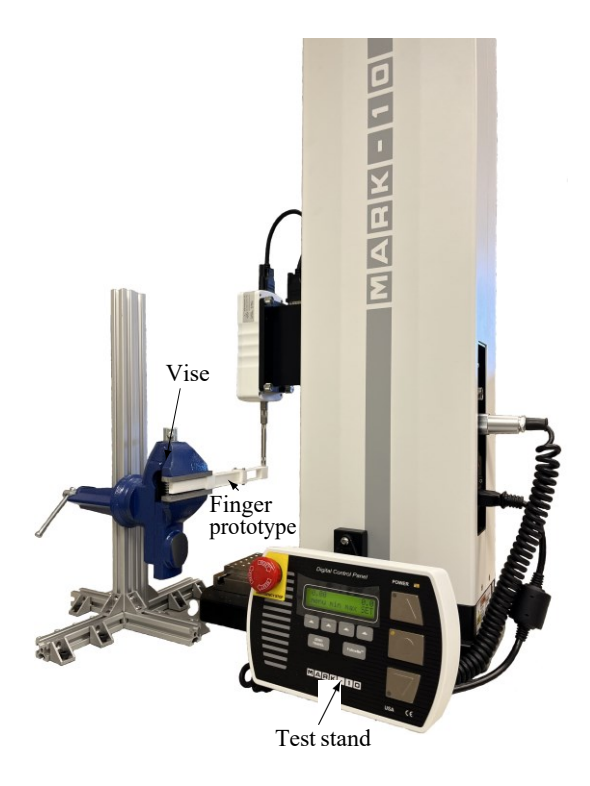


FIGURE 6. EXPERIMENTAL SETUP.

Fig. 7 shows the fitted lines of the experimental data. But it can be seen that when λ is large, the linear relationship between the applied force and deformation is getting worse due to the major difference between the beginning period and the rest deformation process, meaning the stiffness k is no longer a constant. This is mainly due to the artificial setting of the assembly clearance during the production of the finger. When λ is small, the impact of these clearances on the overall deformation is negligible as a percentage. However, when λ is large, the overall

deformation becomes smaller, and the clearances have a significant impact on the overall deformation.

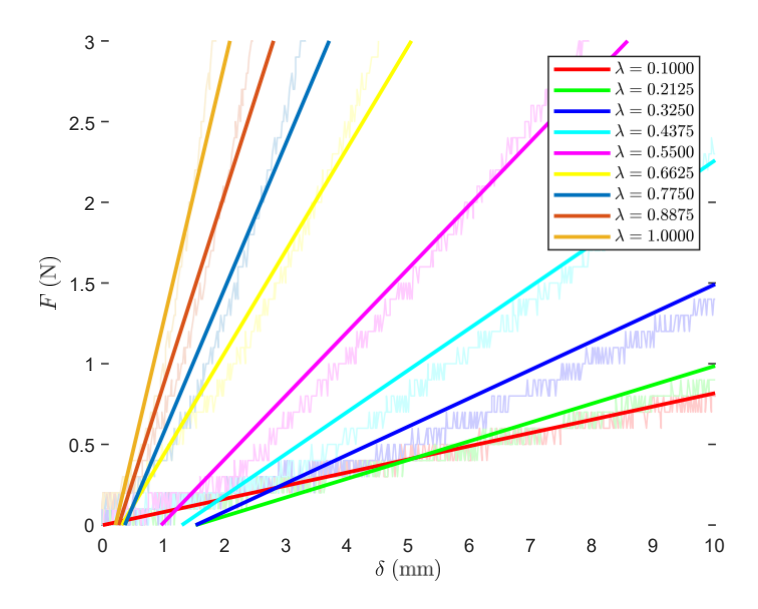


FIGURE 7. RESULTS OF THE EXPERIMENTAL TEST WITH DIFFERENT SLIDER-FILLING RATIO λ .

Stiffness at different λ is obtained by linearly fitting the force and deformation. The results are compared between the theoretical model and the FEA method, as shown in Fig. 8. Although changing of λ is equally spaced, the corresponding change of stiffness is not linear. The larger the λ is, the greater the changing of stiffness will be. The stiffness range ratios of the theoretical method and FEA method are 140.85 and 142.45 respectively. But the stiffness range ratio of the experimental test is 19.62. It is noticed that the theoretical model and the FEA method have the similar results, and the empiric stiffness is lower than those from the other two methods, especially when λ is greater than 0.5. Assembly clearance is a factor in this effect. In order to eliminate as much as possible its influence on the measurement error, the original data that with the force larger than 2 N are used to fit. The slopes of the new lines are chosen as the stiffness and add them to Fig. 8 for comparison with other results. It can be seen that the stiffness has improved significantly when the λ is large, and the stiffness ratio reaches 36.94. But there is still some gap compared to the theoretical model and FEA, which is the result of not completely eliminating the clearance of the assembly clearance.

Even with the current imperfect finger prototype, it still has good variable stiffness performance. For example, for an egg weighing 55 g, the stiffness can be adjusted to the minimum, which will result in a deformation of the finger of about 6.5 mm.

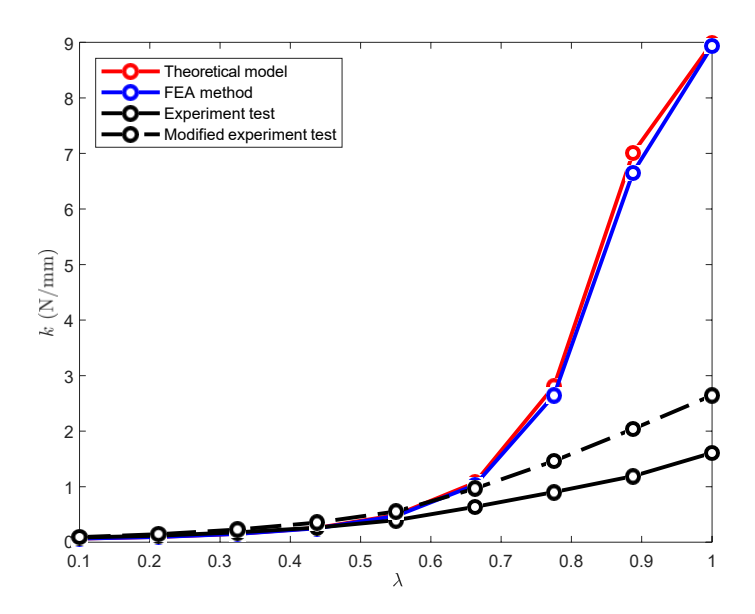


FIGURE 8. STIFFNESS VARYING WITH DIFFERENT SLIDER-FILLING RATIO λ .

But for a stainless steel cup weighing 500 g, the stiffness can be adjusted to the maximum, where the deformation is only about 3 mm. This finger can cope with light and fragile objects, as well as heavy and sturdy objects in daily life. For the former, λ is best selected in the range 0.1 to 0.7, while for the latter, λ can be selected in the range 0.8 to 1.0.

4.2 Gripping Demonstration

In order to demonstrate the wide applicability of the gripper using such fingers, several daily objects are selected, including a potato chip, an empty bottle, a sponge, an orange, and a striped metal block. Different grasping strategies are adopted for different objects, as shown in Fig. 9. The Chip and empty bottle are light and easily deformed, so the stiffness is adjusted to the minimum. The sponge is very light but not so fragile, so the stiffness can be adjusted slightly higher. The orange is heavier, but in order to avoid damage to its surface, the stiffness is not adjusted too large. The metal block is heavy and does not deform easily, so the maximum stiffness can be chosen.

5 CONCLUSIONS

In this paper, a new variable-stiffness robotic finger is proposed. The design allows the compliance to be changed by continuously changing the filling ratio of the finger cavity inside a parallel beam mechanism. This mechanism can be driven directly by servo motors and can quickly change the stiffness to adapt to new environments in a short time with large stiffness

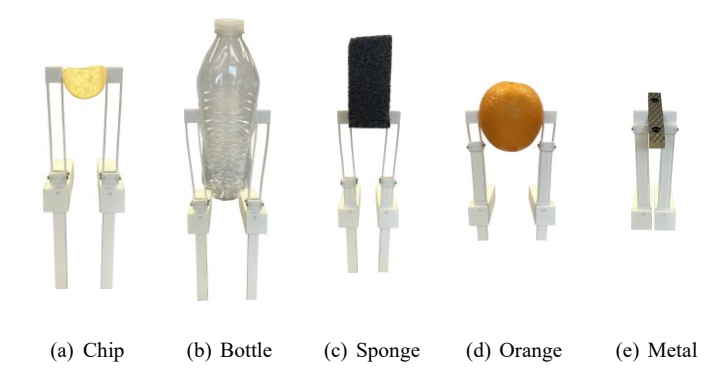


FIGURE 9. OBJECTS FOR DEMONSTRATING ADAPTIVE GRASPING

change ratio (around 1:37 based on the tested prototype). A theoretical model of this mechanism was developed, and validated with the FEA results with stiffness error less than 6.43%. The effect of multiple design parameters on the stiffness of the finger was investigated and optimal parameters could be selected based on the analysis. Then a finger prototype was manufactured to further investigate the performance of the finger through experiments. At a lower filling ratio, the experimental prototype and the theoretical model agreed well, but when the filling ratio is higher, the error increased due to the manufacturing and assembly errors. The function performance of the designed gripper was demonstrated by a group of various representative daily objects. Experiments showed the potential of the finger for a large range of stiffness variation in flexible grasping. Future work is to further improve the accuracy of the theoretical model and the process of finger prototyping to reduce errors caused by machining and assembly. A complete actuated gripper is going to be developed with automatic grasping tests and validation. The long-term goal is to apply this gripper to industrial and domestic robotic grasping and manipulation applications by providing a cost-effective and efficient solution.

ACKNOWLEDGMENT

This work was funded by the National Science Foundation (NSF) grant under FRR-2131711.

REFERENCES

- [1] Siciliano, B., and Khatib, O., 2016. "Robotics and the handbook". In *Springer Handbook of Robotics*. Springer, pp. 1–6.
- [2] Armanini, C., Hussain, I., Iqbal, M. Z., Gan, D., Prattichizzo, D., and Renda, F., 2021. "Discrete cosserat ap-

- proach for closed-chain soft robots: Application to the finray finger". *IEEE Transactions on Robotics*, **37**(6), pp. 2083–2098.
- [3] Hussain, I., Malvezzi, M., Gan, D., Iqbal, Z., Seneviratne, L., Prattichizzo, D., and Renda, F., 2021. "Compliant gripper design, prototyping, and modeling using screw theory formulation". *The International Journal of Robotics Re*search, 40(1), pp. 55–71.
- [4] Anwar, M., Al Khawli, T., Hussain, I., Gan, D., and Renda, F., 2019. "Modeling and prototyping of a soft closed-chain modular gripper". *Industrial Robot: the international journal of robotics research and application*.
- [5] Kim, S., Laschi, C., and Trimmer, B., 2013. "Soft robotics: a bioinspired evolution in robotics". *Trends in biotechnology*, **31**(5), pp. 287–294.
- [6] Catalano, M. G., Grioli, G., Farnioli, E., Serio, A., Piazza, C., and Bicchi, A., 2014. "Adaptive synergies for the design and control of the pisa/iit softhand". *The International Journal of Robotics Research*, **33**(5), pp. 768–782.
- [7] Deimel, R., and Brock, O., 2016. "A novel type of compliant and underactuated robotic hand for dexterous grasping". *The International Journal of Robotics Research*, **35**(1-3), pp. 161–185.
- [8] Rus, D., and Tolley, M. T., 2015. "Design, fabrication and control of soft robots". *Nature*, **521**(7553), pp. 467–475.
- [9] Manti, M., Hassan, T., Passetti, G., D'Elia, N., Laschi, C., and Cianchetti, M., 2015. "A bioinspired soft robotic gripper for adaptable and effective grasping". *Soft Robotics*, 2(3), pp. 107–116.
- [10] Homberg, B. S., Katzschmann, R. K., Dogar, M. R., and Rus, D., 2015. "Haptic identification of objects using a modular soft robotic gripper". In 2015 IEEE/RSJ International Conference on Intelligent Robots and Systems (IROS), IEEE, pp. 1698–1705.
- [11] Dai, J., Zhu, M., and Feng, Y., 2021. "Stiffness control for a soft robotic finger based on reinforcement learning for robust grasping". In 2021 27th International Conference on Mechatronics and Machine Vision in Practice (M2VIP), IEEE, pp. 540–545.
- [12] Nagase, J.-y., Wakimoto, S., Satoh, T., Saga, N., and Suzumori, K., 2011. "Design of a variable-stiffness robotic hand using pneumatic soft rubber actuators". *Smart Materials and Structures*, **20**(10), p. 105015.
- [13] Takashima, K., Sugitani, K., Morimoto, N., Sakaguchi, S., Noritsugu, T., and Mukai, T., 2014. "Pneumatic artificial rubber muscle using shape-memory polymer sheet with embedded electrical heating wire". *Smart Materials and Structures*, **23**(12), p. 125005.
- [14] Hussain, I., Al-Ketan, O., Renda, F., Malvezzi, M., Prattichizzo, D., Seneviratne, L., Abu Al-Rub, R. K., and Gan, D., 2020. "Design and prototyping soft-rigid tendon-driven modular grippers using interpenetrating phase com-

- posites materials". *The International Journal of Robotics Research*, **39**(14), pp. 1635–1646.
- [15] Majidi, C., and Wood, R. J., 2010. "Tunable elastic stiffness with microconfined magnetorheological domains at low magnetic field". *Applied Physics Letters*, **97**(16), p. 164104.
- [16] Taniguchi, H., Miyake, M., and Suzumori, K., 2010. "Development of new soft actuator using magnetic intelligent fluids for flexible walking robot". In ICCAS 2010, IEEE, pp. 1797–1801.
- [17] Shintake, J., Schubert, B., Rosset, S., Shea, H., and Floreano, D., 2015. "Variable stiffness actuator for soft robotics using dielectric elastomer and low-melting-point alloy". In 2015 IEEE/RSJ International Conference on Intelligent Robots and Systems (IROS), IEEE, pp. 1097–1102.
- [18] Al-Rubaiai, M., Pinto, T., Qian, C., and Tan, X., 2019. "Soft actuators with stiffness and shape modulation using 3d-printed conductive polylactic acid material". *Soft robotics*, **6**(3), pp. 318–332.
- [19] Firouzeh, A., Salerno, M., and Paik, J., 2017. "Stiffness control with shape memory polymer in underactuated robotic origamis". *IEEE Transactions on Robotics*, **33**(4), pp. 765–777.
- [20] Al Abeach, L. A., Nefti-Meziani, S., and Davis, S., 2017. "Design of a variable stiffness soft dexterous gripper". Soft robotics, 4(3), pp. 274–284.
- [21] Zhu, H., Li, X., Chen, W., and Zhang, C., 2019. "Flexure-based variable stiffness gripper for large-scale grasping force regulation with vision". In International Conference on Intelligent Robotics and Applications, Springer, pp. 346–357.
- [22] Kim, Y.-J., Cheng, S., Kim, S., and Iagnemma, K., 2013. "A novel layer jamming mechanism with tunable stiffness capability for minimally invasive surgery". *IEEE Transactions on Robotics*, **29**(4), pp. 1031–1042.
- [23] Li, Y., Chen, Y., Yang, Y., and Wei, Y., 2017. "Passive particle jamming and its stiffening of soft robotic grippers". *IEEE Transactions on robotics*, **33**(2), pp. 446–455.
- [24] Chandrasekaran, K., Somayaji, A., and Thondiyath, A., 2021. "A novel design for a compliant mechanism based variable stiffness grasper through structure modulation". *Journal of Medical Devices*, 15(1), p. 014501.
- [25] Li, X., Chen, W., Lin, W., and Low, K. H., 2017. "A variable stiffness robotic gripper based on structure-controlled principle". *IEEE Transactions on Automation Science and Engineering*, **15**(3), pp. 1104–1113.
- [26] Melchiorri, C., Palli, G., Berselli, G., and Vassura, G., 2013. "Development of the ub hand iv: Overview of design solutions and enabling technologies". *IEEE Robotics & Automation Magazine*, **20**(3), pp. 72–81.
- [27] Kim, Y.-J., Cheng, S., Kim, S., and Iagnemma, K., 2013. "A stiffness-adjustable hyperredundant manipulator using

- a variable neutral-line mechanism for minimally invasive surgery". *IEEE transactions on robotics,* **30**(2), pp. 382–395
- [28] Fu, J., and Gan, D., 2021. "A reconfigurable variable-stiffness parallel beam for compliant robotic mechanisms towards safe human interaction". In International Design Engineering Technical Conferences and Computers and Information in Engineering Conference, Vol. 85444, American Society of Mechanical Engineers, p. V08AT08A020.
- [29] Awtar, S., Slocum, A. H., and Sevincer, E., 2007. "Characteristics of beam-based flexure modules".
- [30] Awtar, S., Shimotsu, K., and Sen, S., 2010. "Elastic averaging in flexure mechanisms: A three-beam parallelogram flexure case study".